Electronic Supplementary Information

Structure and Magnetism of a Binuclear Cu^{II} Pyrophosphate: Transition to a 3D Magnetic Behaviour Studied by Single Crystal EPR

Rosana P. Sartoris, Otaciro R. Nascimento, Ricardo C. Santana, MireillePerec, Ricardo F. Baggio and Rafael Calvo

Fig. S1: Full set of spectra observed between 4.7 and 50 K for the magnetic field applied at 132° with the ***x*** axis in the *xy* laboratory plane, as shown in the inset of Figure 4.

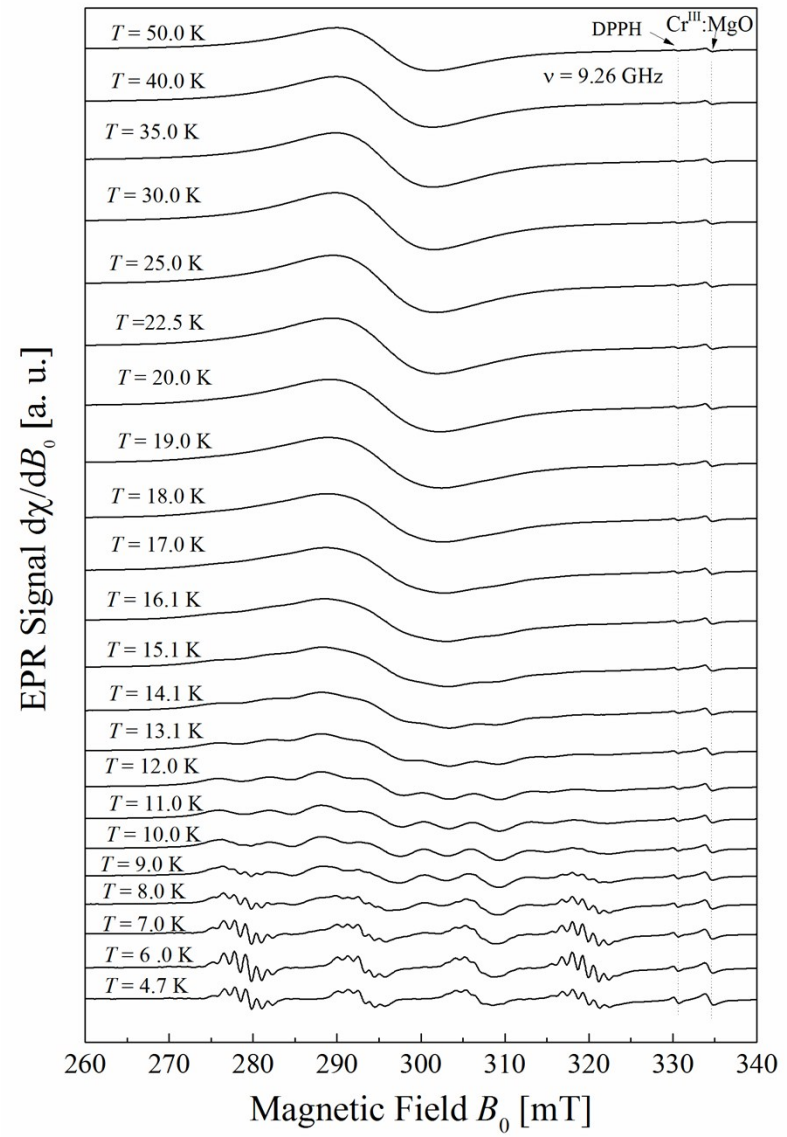

Fig. S2: Enlarged view of Figure 4a showing the dinuclear hyperfine splitting of the copper resonance at 4.7 K (black line) for the magnetic field orientate in the xy plane at 132° of the x axes. The red lines are simulated with the components of the $\boldsymbol{g}_{M1}$ and $\boldsymbol{A}_{M1}$ matrices given in Table 5 and assuming A_{N1}= 8.7 10^{-4} cm^{-1} and A_{N2} = 12 10^{-4} cm^{-1}. The red vertical line in the inset a) and b) indicates the field orientation where the data were obtained.

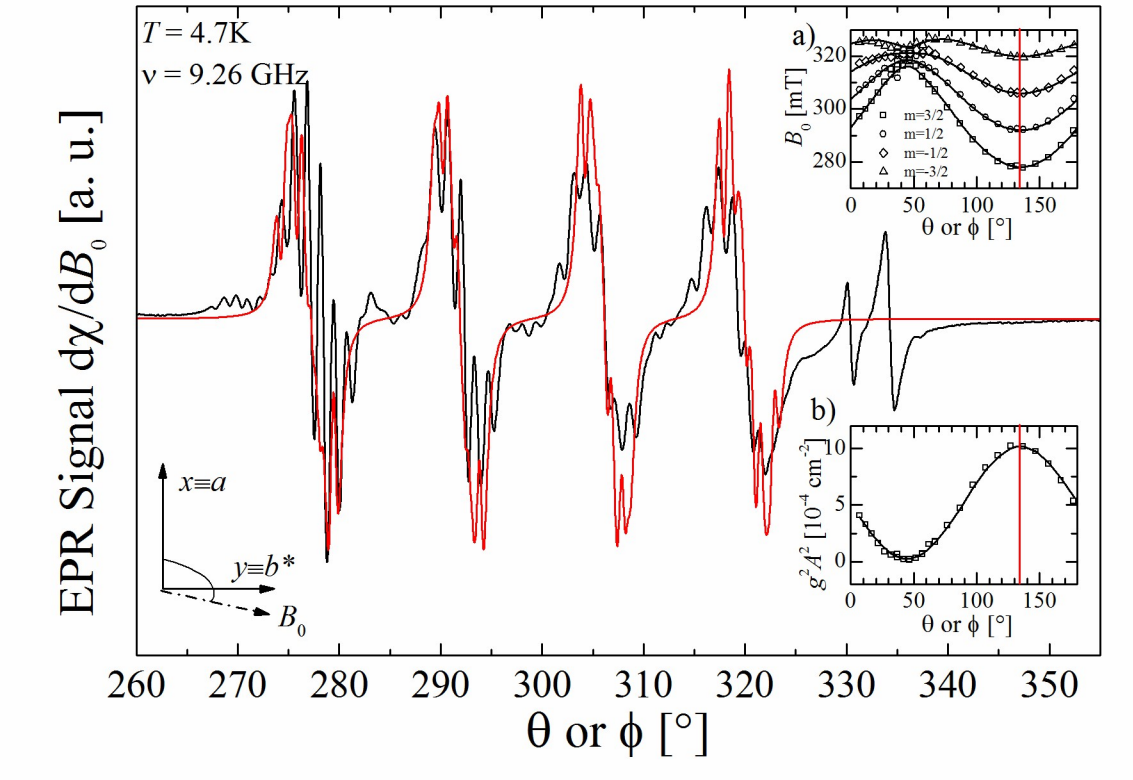

Fig. S3: Enlarged view of Figure 4d showing the dinuclear hyperfine splitting of the copper resonance at 12 K for the magnetic field orientation described in the inset of Figure 4. The resolution is poorer for other orientations of B_0. The dinuclear spectra (red line) are simulated using Easyspin, a package of programs working under Matlab. The peak indicated with a red arrow is the high field peak of the mononuclear site M_1.

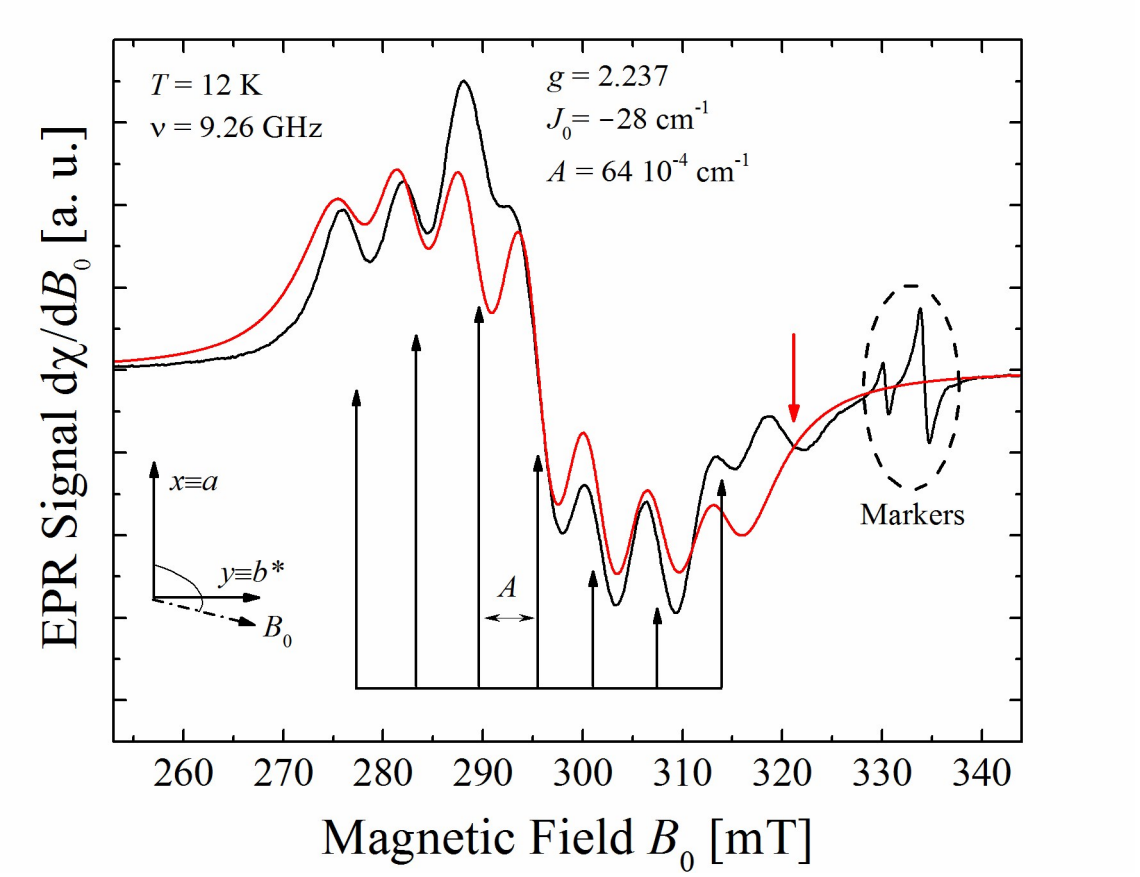

Fig. S4: Angular variation of the field position of the copper hyperfine transitions observed for the site M_2 in the three planes of the *xyz* laboratory system. The red stars in a) indicate the centers of the copper hyperfine groups of the site M_1. The uncertainties are much larger than those for site M_1, displayed in Figure 6.

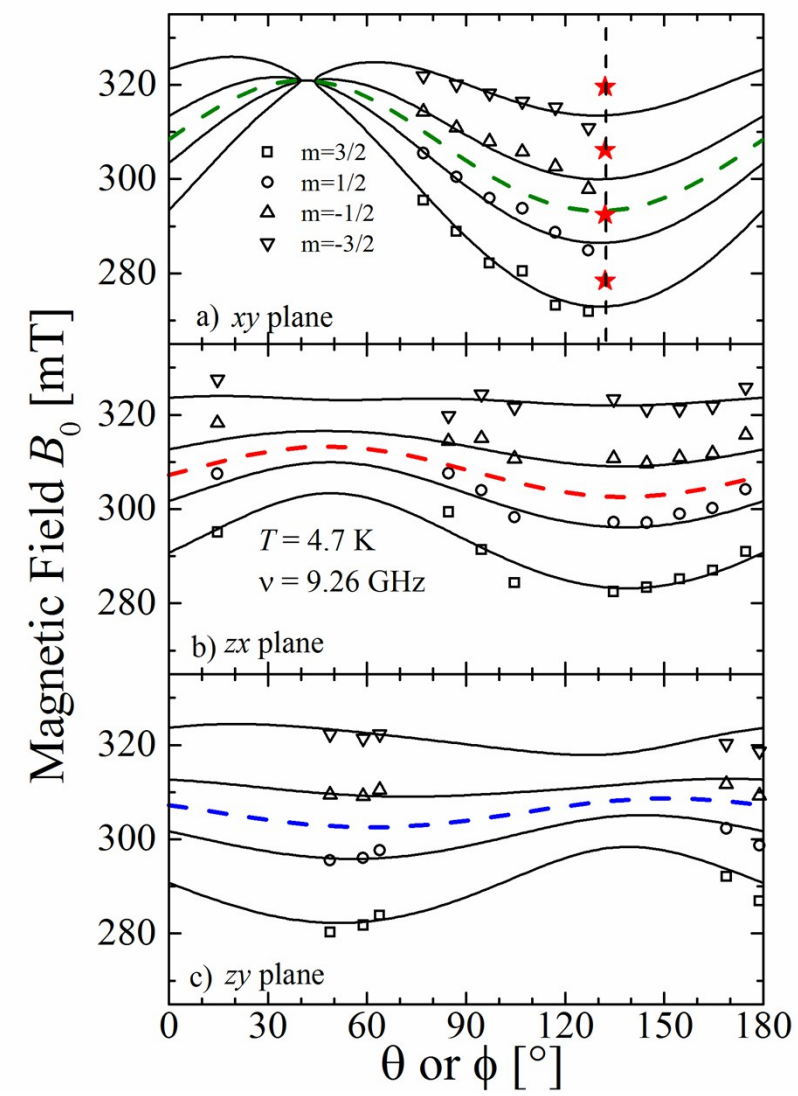

Fig. S5 Values of g^2 (a) and g^2A^2 (b) calculated from the field positions shown in Figure S3 for the mononuclear site M_2. The solid lines are obtained with the $\boldsymbol{g}_{M2}$ and $\boldsymbol{A}_{M2}$ matrices given in Table S1. The uncertainties are much larger than those for site M_1, displayed in Figure 7.

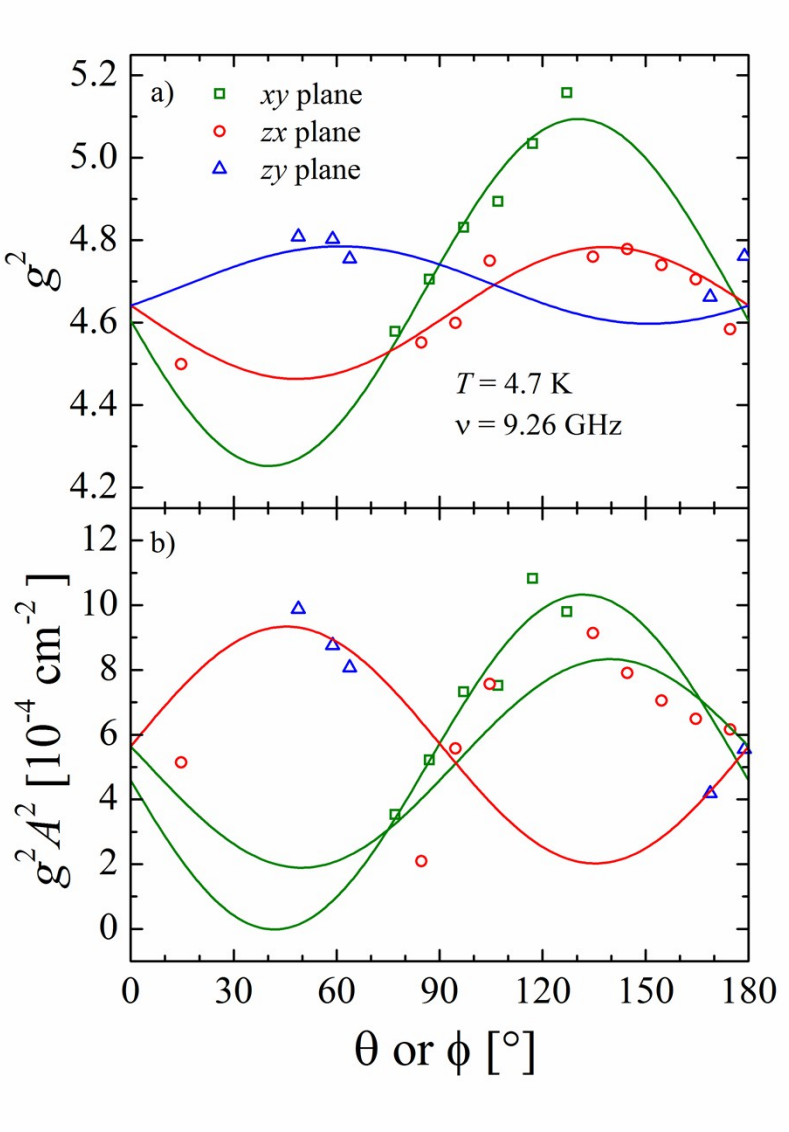

Fig S6: Double integration of the signal observed for allowed ($\Delta M_S = 1$) and forbidden ($\Delta M_S = 2$) transitions in the relevant field ranges. The jumps of this integral corresponds to the areas of these peaks, that are related by a factor of ~1000.

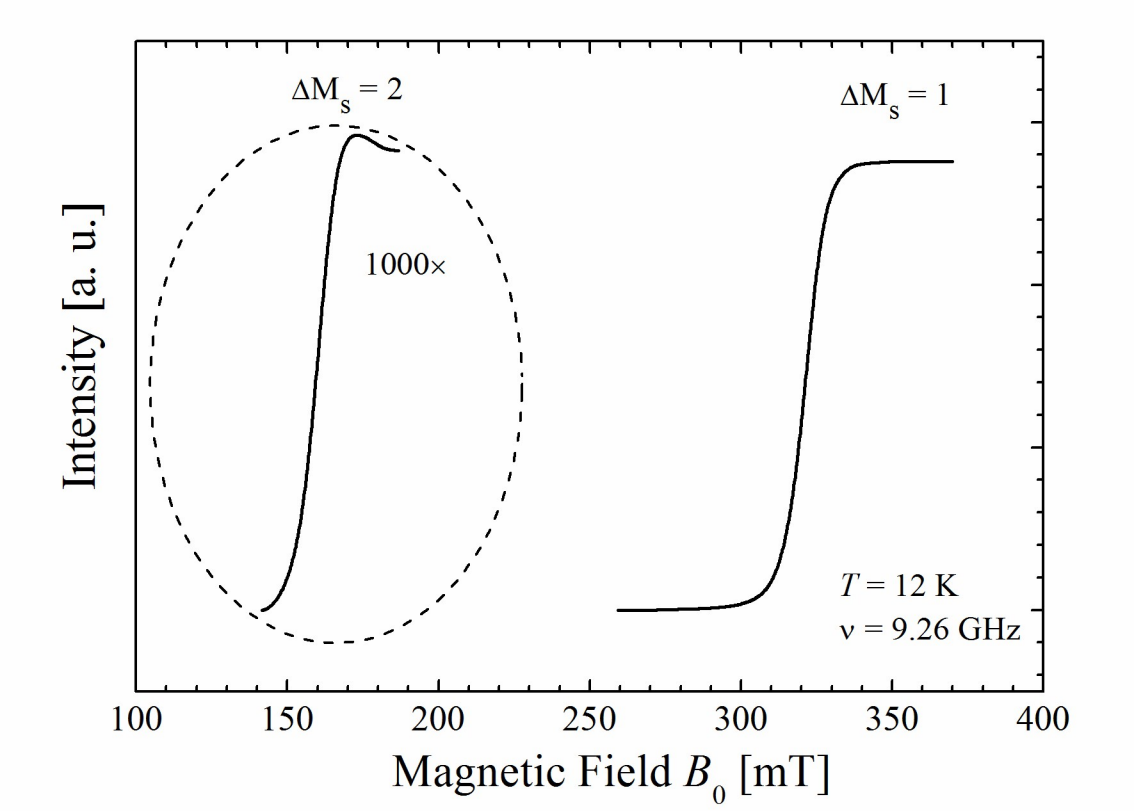

Fig. S7 Full set of spectra observed around 160 mT and *T* between 4 and 50 K for the magnetic field applied at 70° with the ***x*** axis in the *xy* laboratory plane, as indicated with the arrow in the Figure 8.

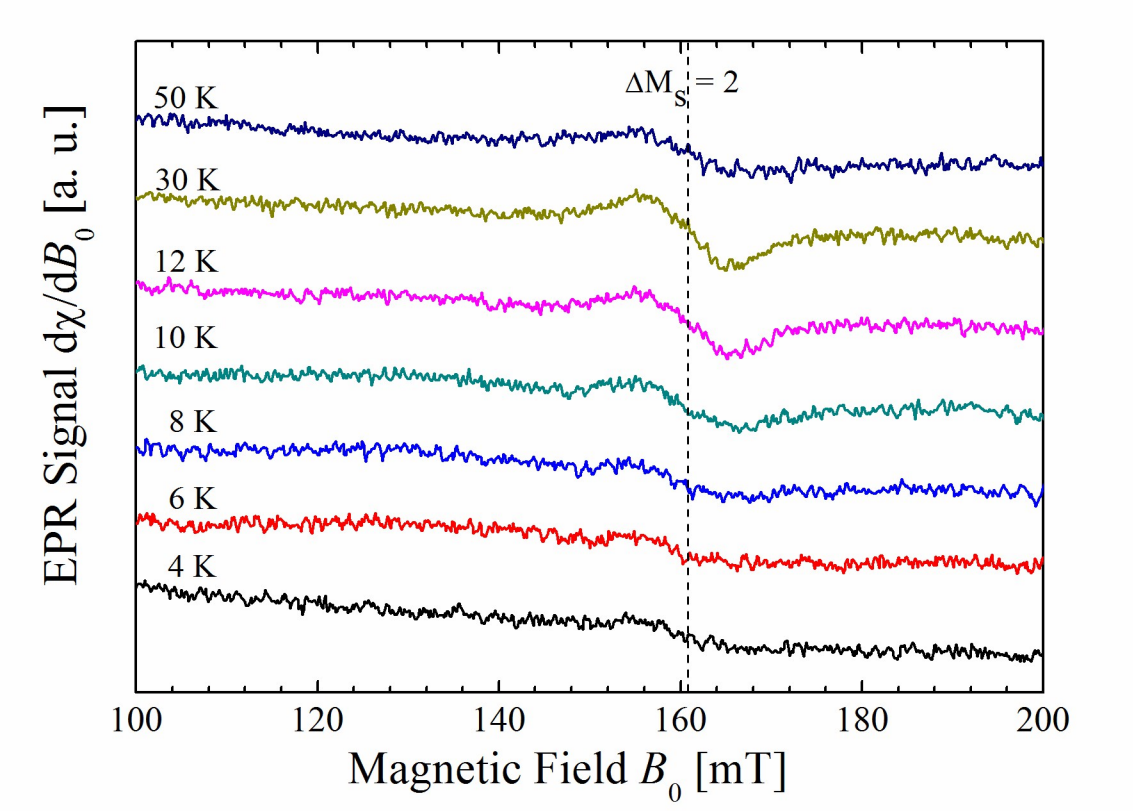

Table S1: Eigenvalues and eigenvectors of the $\boldsymbol{g}_{\mathbf{M2}}$ and $\boldsymbol{A}_{\mathbf{M2}}$ matrices of mononuclear site M_2, calculated from the EPR results at 4.7 K in Figures S3 and S4.

	Eigenvalues	Eigenvectors		
g_1	2.06(8)	0.77(1)	0.60(4)	0.18(8)
g_2	2.014(5)	−0.06(8)	0.36(4)	−0.93(1)
g_3	2.269(4)	−0.63(1)	0.71(1)	0.31(1)
A_1	80(10) 10^{-4} cm^{-1}	0.73(5)	0.67(5)	−0.0(1)
A_2	0(20) 10^{-4} cm^{-1}	−0.4(1)	0.4(1)	−0.84(2)
A3	160(10) 10^{-4} cm^{-1}	−0.56(2)	0.63(2)	0.53(2)